S-345

# RESEARCH ARTICLE

## Ultrasound image smoothing based on adaptive and non-adaptive filters

Heba Khudhair Abbas<sup>1</sup>, Haidar Jawad Mohamad<sup>2</sup>, Khloud Falih Abbas<sup>3</sup>

#### **Abstract**

**Objective:** To model adaptive and non-adaptive filters to ensure smooth ultrasound images.

**Method:** The comparative study was conducted at Al-Yarmouk Teaching Hospital, Al Mustansiriyah University, Baghdad, Iraq, in 2019, and comprised ultrasound images of kidney (303x208 pixel) and foetus (111x109 pixel). These images were smoothed based on 8 filters; 1 non-adaptive (median), and 7 adaptive enhanced filters (Gamma, Wiener, Lee, Frost, Kuan, Adaptive Lee and Adaptive Frost). They were applied to the images by windows measuring 3x3, 5x5, 7x7. The additive noise and the multiplicative noise factor were calculated using histogram to determine the noise type for each image. Statistical criteria included mean square error, normalised absolute error and signal-to-noise ratio.

**Result:** The relationship between noise ratio and filter type showed that Wiener was the best filter and the best sliding window was 3x3. The worst filters were Gamma, EFrost and Kuan.

**Conclusion:** The relationship between sliding window size and noise ratio for all the smoothing filters clearly identified the best filter for the type of noise.

**Key Words:** Kidney, Fetus, Ultrasonography, Smoothing

(JPMA 74: S345 (Supple-8); 2024) DOI: https://doi.org/10.47391/JPMA-BAGH-16-79

## Introduction

Digital images are used as information source in many research fields<sup>1,2</sup>. Unfortunately, similar to other digital signals, digital images are also sometimes unintentionally corrupted by unwanted signals, called noise<sup>3,4</sup>. Digital images play an important role both in daily life applications, such as satellite television and medical imaging<sup>5,6</sup>, as well as in areas of research and technology, such as geographical information systems (GIS) and astronomy<sup>7</sup>. Digital images are often corrupted by different types of noise during the acquisition and transmission phases<sup>8,9</sup>. Such degradation negatively influences the performance of many image processing techniques, and a pre-processing module to filter the images is often required<sup>10</sup>. Noise removal is one of the major concerns in the field of computer vision and image processing. The goal of removing noise is primarily to suppress the noise as well as to preserve the integrity of edges and detailed information<sup>11</sup>. In the field of digital image processing, two applications of great importance are noise filtering and image enhancement<sup>12</sup>. A model of speckle noise reduction with various filters is basically used for speckle elimination. Smoothing or elimination of speckle noise in medical ultrasound images have been

<sup>1</sup>Department of Physics, University of Baghdad, Baghdad, Iraq<sup>2</sup> Department of Physics, Mustansiriyah University. Baghdad, Iraq.<sup>3</sup> Department of Physiology, Mustansiriyah University. Baghdad, Iraq.

Correspondence: Heba Khudhair Abbas Email: Haidar.mohamad@uomustansiriyah.edu.iq studied in details such as spatial filtering, diffusion filtering, and wavelet filtering. For instance, Manoj et al.<sup>13</sup> used computed tomography (CT) images to manage the noise using Bayes shrinkage rule in Shearlet domain. Hyunho et al.<sup>14</sup> studied speckle-reducing anisotropic diffusion (SRAD) and a Bayes threshold in the wavelet domain. They used signal-to-noise ratio (SNR) to show the quality of the enhancement algorithm as a criterion. Carlos et al.<sup>15</sup> used full-reference distortion metrics and filter evaluation process to have ouput certainty.

The current study was planned to model adaptive and non-adaptive filters to ensure smooth ultrasound images.

## **Materials and Methods**

The comparative study was conducted at Al-Yarmouk Teaching Hospital, Al Mustansiriyah University, Baghdad, Iraq, in 2019, and comprised ultrasound images of kidney (303x208 pixel) and foetus (111x109 pixel). These images were smoothed based on 8 filters; 1 non-adaptive (median), and 7 adaptive enhanced filters (Gamma, Wiener, Lee, Frost, Kuan, Adaptive Lee and Adaptive Frost). They were applied to the images by windows measuring 3x3, 5x5, 7x7. Methods of noise removal can be both linear and non-linear. Linear methods are fast enough, but do not preserve image detail, and nonlinear methods preserve image detail. De-noising filters (smoothing techniques) can be classified into two kinds of filters: non-adaptive filters which can directly apply to the noisy images without the need for any prior knowledge on the statistical relationship governing the image The 16th scientific international conference S-346

points<sup>16,17</sup>, and adaptive filters that are used to smooth speckle multiplicative noise in ultrasound images<sup>18,19</sup>.

Wiener filter involves linear estimation of a desired image data sequence from another related sequence. Wiener method implements spatial smoothing and its model complexity control corresponds to the window size. Lee's filter exploits the local statistics within the image region to reduce both additive and multiplicative noise in different images.

Additive noise smoothing filter has the model: I(x,y)=R(x,y)+n(x,y) in which I(x,y), R(x,y), and n(x,y) represent the observed image, and the original with mean value equal to zero, respectively.

However, small window size results in an undesirable smoothing. It is our opinion, that 3x3 or 5x5 or 7x7 window sizes are the most effective, and if the noise reduction is not significant, the filter can be run recursively.

Multiplicative noise smoothing filter mathematically is presented by the equation I(x,y) = R(x,y).F(x,y) in which I(x,y) and R(xy) define earlier and F(x,y) represents the signal independent multiplicative noise.

An optimal linear approximation can be used to produce a new filtration algorithm similar to that adopted by additive noise model. This linear approximation can be introduced as  $^{20}$  I(x,y) = R(x,y) F+R(x,y).(F(x,y)-F in which F represents the mean of the multiplicative noise. The priori mean and variance of R(x,y) can, then, be approximated by

$$R x, y = \frac{I x, y}{F}$$

and

Q x,y = 
$$\frac{\sigma_I^2 x,y - I^2 x,y}{\sigma_F^2 - F^2}$$
 - R<sup>2</sup>

in which  $\overline{I}(x, y)$  and  $\sigma_{-}I^2(x, y)$  represent the local mean and the local variances of I(x, y), while  $\sigma_{-}F^2$  is the noise variance. Substitutions in the equation lead to the approximation of the ungraded image with

R (x,y) = R (x,y) + K(x,y)[I x,y - R x,y . Fin which
$$K x,y = \frac{Q x,y . F}{R^2 x.y . \sigma_r^2 + F^2 O x.y}$$

In fact, Luis et al.<sup>21</sup> modified the mentioned filters by adding another improvement factor to improve the smoothing process by incorporating the local gradient information to decide as to which part of the utilised window the centre point belonged.

Kuan filter is a local linear minimum mean square error (LLMMSE) filter based on the non-stationary mean and non-stationary variance (NMNV) image model. While the NM describes the gross structures in an image, the NV characterises the edge structures and the elementary textured information within the image. The observed image, by Kuan's model is:

I(x,y)=R(x,y)+n(x,y) in which n(x,y) is zero mean noise, which can be considered signal-dependent or signal-independent. However, the local linear minimum mean square error (MSE) filter estimates the smooth value in an ultrasound image by<sup>22</sup>:

 $R^{(x,y)}=R^{(x,y)}+ [K_R K]_{-}I^{(-1)}[I(x,y)-I^{(x,y)}]$  in which KRI and KI represent the cross-covariance matrix of R(x,y) and I(x,y), and the covariance matrix of I(x,y), respectively. This filter can be implemented to reduce image noise of both signal-independent and signal-dependent types.

Using the the equation

$$\begin{array}{rcl} R \ x,y \ = & k_1 k_2 C_1^2 \ x,y \ I \ l,k \ e^{-k_2 C_1^2} \ x,y \ x - \ l \ + \ y - \ k \\ & \underset{l = x - \frac{n-1}{2}}{\text{k=y-}} \frac{n-1}{2} \end{array}$$

, the requirements for performing this filter is achieved by determining the local coefficient of variation, i.e. CI(x, y),

$$C_{w} x, y = \frac{\sigma_{w} x, y}{w x, y}$$

in which w(x,y) and  $\sigma_w(x,y)$  represent, respectively, the mean and standard deviation (SD) of the considered random variables (x,y). This parameter, however, can be used as an indicator for the homogeneity of regions within the ultrasound images, and, therefore, can be utilised to control the speckle reduction process in an adaptive smoothing filter.

The designed algorithm in Matlab software for all smoothing filters has 7 steps: Step 1: load ultrasound image (I)= imread(img). Step2: Passing the smoothing filter over the image(I). J = smooth filter (I, [sz sz]); where sz is filter window size. Step4: Calculate the additive noise between the filtered image and the original image using additive noise factor=I-J. Step5: Calculate the multiplicative noise between the filtered image and the

J Pak Med Assoc (Suppl. 8) Open Access

original image using multiplicative noise factor=I. /J. Step6: Plot histogram image for original image and filtering image imhist (I or J). Step7: Plot histogram for additive and multiplicative noise hist (N) where N= noise type.

There are objective evaluations for judging the effect of noise reduction to evaluate the quality of the performance of each filtering method, and the differences between the original image g(x, y) and the filtered image f(x,y) can be quantified by many parameters, such as MSE, which can be expressed by the equation<sup>23</sup>:

MSE = 
$$1/(m \times n) \sum_{x \in \mathbb{Z}} (x = 1)^m \sum_{y \in \mathbb{Z}} (y = 1)^n \| \| ((f(x, y) - g^{(x, y)}) \|^2) \|$$

in which  $g^{(x,y)}$  is processed image after noise reduction from noise-polluted image g(x,y), and it should be smaller for better noise reduction. The MSE has been widely used to quantify image quality. When it is used alone, it does not correlate strongly enough with perceptual quality. It should be used together with other quality metrics and visual perception  $^{24,25}$ . SNR is calculated as

SNR = 
$$10 \log_{10} \frac{\text{f x, y}^2}{\text{f x, y} - \text{g x, y}^2}$$

in which f(x, y) is pure ideal image not polluted by noise, g(x, y) is captured image polluted by noise, the image size is m rows times n lines. The bigger value of the SNR refers to better noise reduction effect. The SNR has been proved to be a very sensitive test for image degradation, but is completely non-specific. Any small change in image noise by de-speckling would cause an increase in the SNR.

The normalised absolute error (NAE) measure is defined as

NAE = 
$$\frac{\prod_{x=1}^{m} \prod_{y=1}^{n} f x, y - g x, y}{\prod_{x=1}^{m} \prod_{y=1}^{n} f x, y}$$

Large NAE value means de-noised image is of poor quality 26,27

The designed algorithm for the criterion has 7 steps: Step1: Load ultrasound image or added-noise image (img1) and read img1; I1=imread(img1). Step2: Load filtering image (img2) and read img2; I2 =imread(img2). Step3: Display I1 and I2. Step4: Calculate criteria between I1&I2 MSE = immse(I1, I2). Step5: Calculate NAE between I1&I2 NAE = sum(sum((K)))./sum(sum((I1))); where K= imabsdiff(I1, I2) and imabsdiff is function expressing

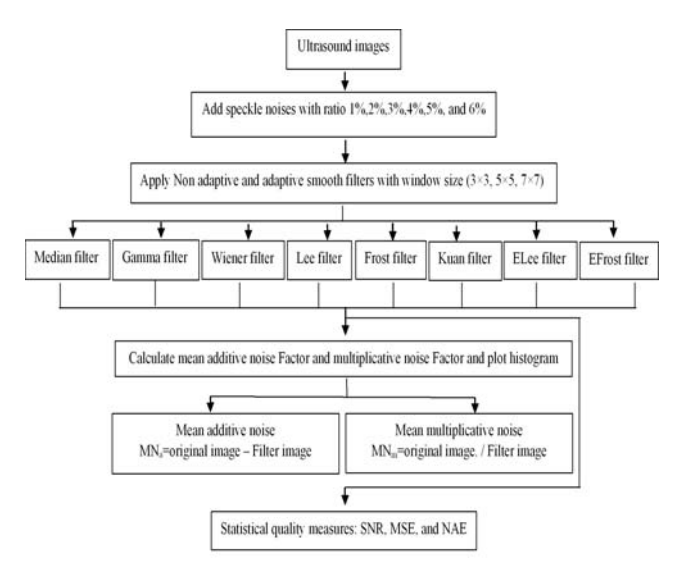


Figure-1: The study flowchart.

MSE: Mean square error, NAE: Normalised absolute error, SNR: Signal-to-noise ratio

absolute difference between two images. Step7: Calculate SNR; snr = snr(I1, I2).

The detailed algorithm was noted (Figure 1).

#### Results

Kidney ultrasound image size was 303x208 pixel with pixel depth 24 bit, and the ultrasound image of foetus was of size 696x486 pixel with pixel depth 24 bit. Surface structures, such as in the foetal image, were at frequency 7-18 MHz to provide better axial and lateral resolution. The kidney image was taken at a frequency of 1-6MHz with lower focal and lateral resolution, but with greater penetration.

Speckle noise was added with per cent from 0.01 to 0.06 to the images used, and the added noise made the image difficult to enhance. Smoothing of the ultrasound images using median, Weiner, Lee, Frost, Kuan filters with window size 3x3, 5x5 and 7x7 showed that the noise smoothing behaviour was the same for all noise per cent in the 3x3 sliding window for both median and Weiner filters for all noise ratios. For sliding window 5x5 and 7x7, the noise behaviour was the same in the image. This behaviour was different with the remaining filters (Figure 2).

Smoothing histogram decreased with the number of pixels in the median, Wiener, Lee and Kuan filters as the filter window size increased. There was increase in the number of pixels in the Frost filters as the size of the filter window increased or the noise ratio increased. Smoothing histogram decreased in the number of pixels in the median, Wiener and Lee filters as the filter window size increased. There was increase in the number of pixels

The 16th scientific international conference S-348

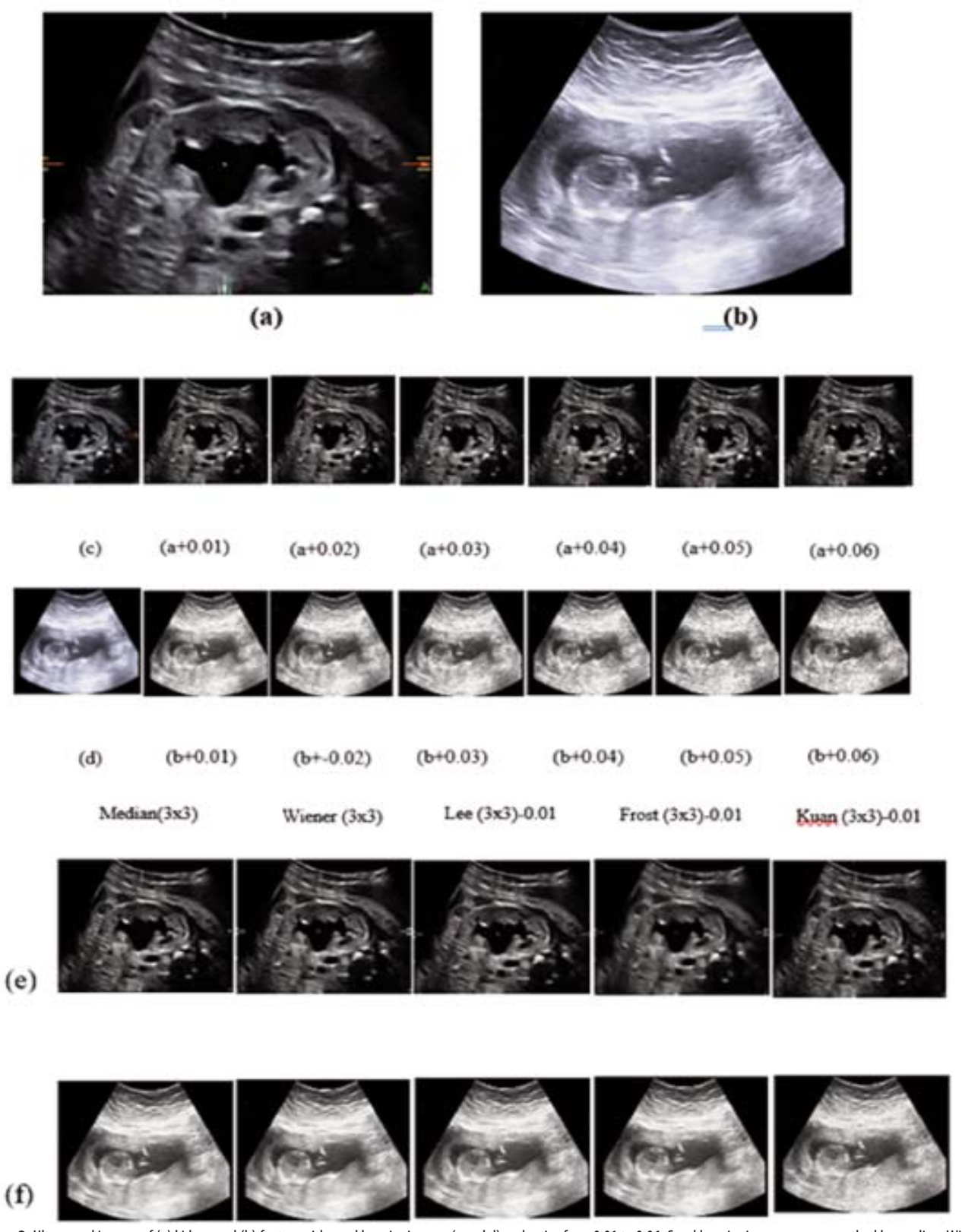


**Figure-2**: Ultrasound images of (a) kidney and (b) foetus, with speckle noise images (c and d) and ratios from 0.01 to 0.06. Speckle noise images were smoothed by median, Wiener, Lee, Frost and Kuan filters for (e) kidney and (f) foetus images.

J Pak Med Assoc (Suppl. 8)

Open Access

S-349

The 16th scientific international conference

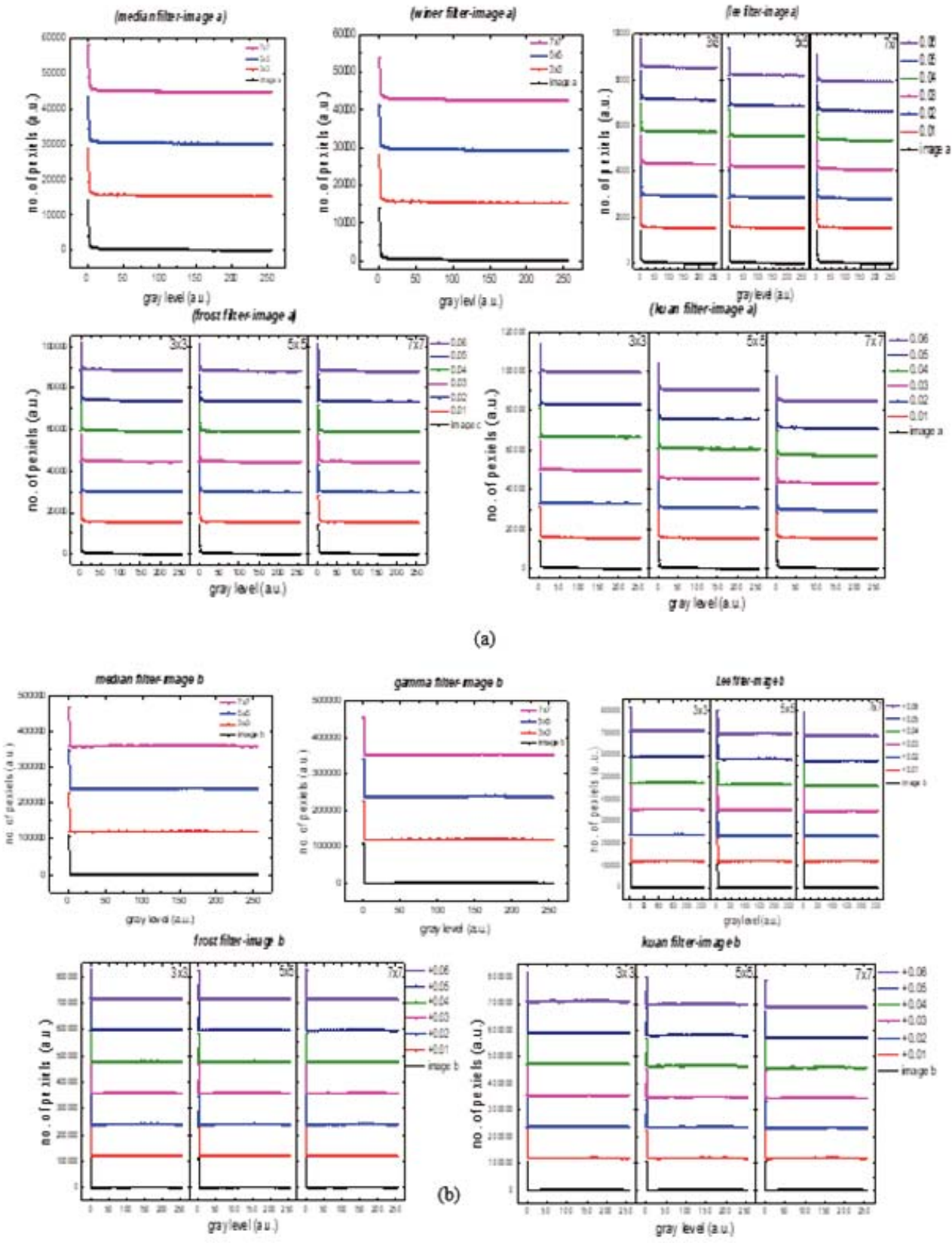


Figure-3: Histogram of the smoothed image with different window sizes.

Open Access Vol. 74, No.10 (Suppl. 8), October 2024

The 16th scientific international conference S-350

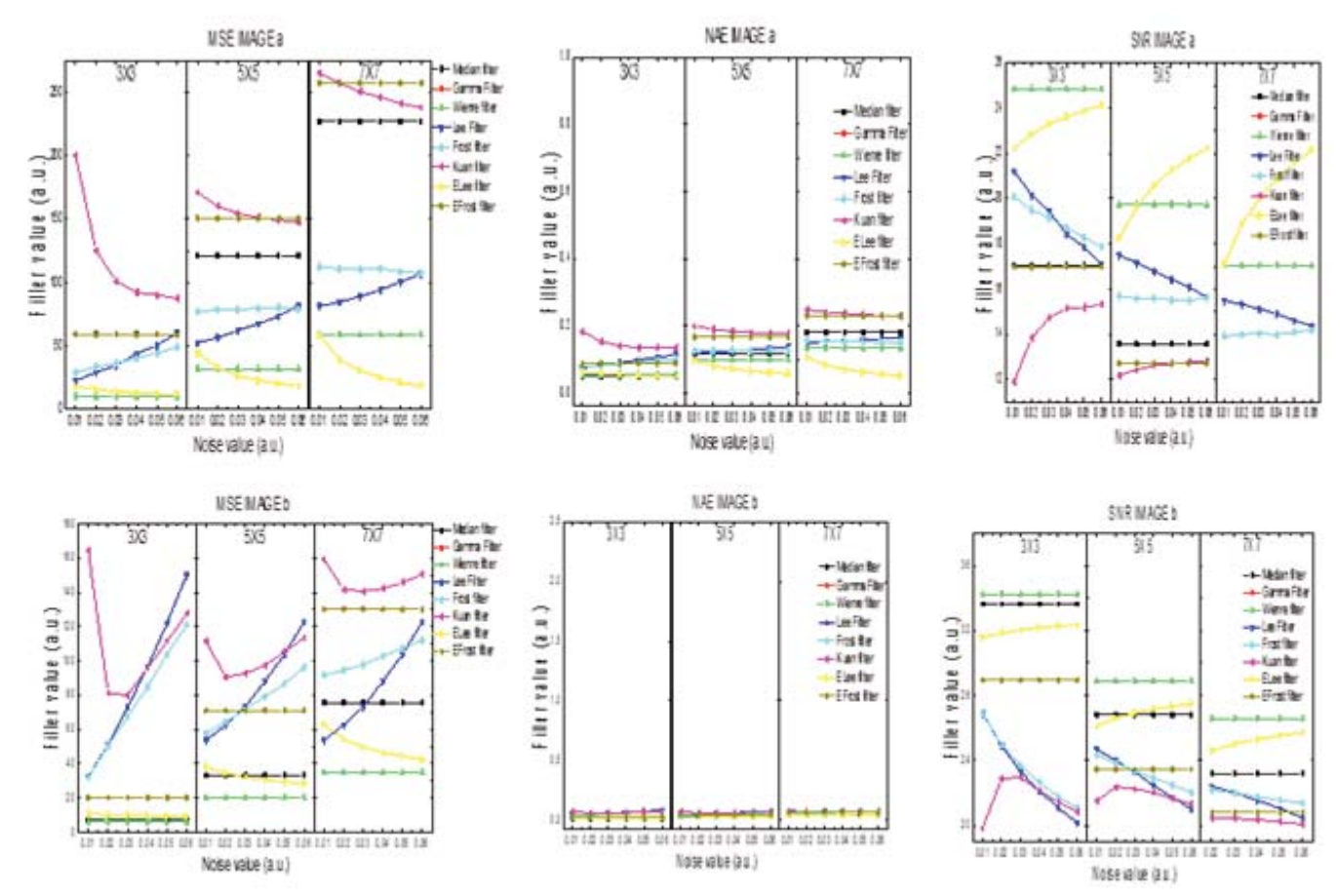


Figure-4: Statistical data with different window sizes.

in the Frost and Kuan filters as the size of the filter window increased or the noise ratio increased (Figure 3).

Statistical data with different window sizes was noted (Figure 4).

#### Discussion

The Wiener filter had lower value than ELee, Lee, Frost, median (3x3), Gamma, EFrost and Kuan using MSE criteria. Median 3x3 had lower value than Wiener, ELee, Lee, Frost, Gamma, EFrost and Kuan using NAE. Wiener had higher value than ELee, Lee, Frost, Median (3x3), Gamma, EFrost and Kuan using SNR.

Wiener had lower value than median (3x3), ELee, Gamma, EFrost, Lee, Frost and Kuan using MSE criteria. Wiener had lower value than median (3x3), ELee, Gamma, EFrost, Lee, Frost and Kuan using NAE. Wiener had higher value than ELee, Lee, Frost, median (3x3), Gamma, EFrost and Kuan using SNR criteria. The results can be compared with other publications, although they used different source of images<sup>9</sup>. They used almost the same filters and same sliding window size which makes it possible to compare

the findings. The behaviour of the sliding windows had the same behaviour<sup>9</sup>.

**Limitation:** The current study has limitations as the sample size was not calculated.

#### Conclusion

The behaviour of the filter changed. The sliding filter window (3x3, 5x5, and 7x7) had some effect on the output of the enhancement. Median, Wiener, Gamma and EFrost filters were unaffected by increased noise ratio in the image, but were affected by the increase in the filter window size. The best results for the criteria were with filter window size 3x3 which had lower values in MSE around 100au and NAE around 1.8au, while it had higher values in SNR around 23au. As the size of the filter window increased, the value of the criteria decreased, indicating that the noise effect was reduced. For MSE, NAE and SNR, the best results came with the lower value of MSE, while SNR gave better results with higher value of the criteria around 23au.

Disclaimer: None.

J Pak Med Assoc (Suppl. 8) Open Access

S-351

The 16th scientific international conference

#### Conflict of Interest: None.

### Source of Funding: None.

#### References

- Mújica-Vargas D, de Jesús Rubio J, Kinani JM, Gallegos-Funes FJ. An efficient nonlinear approach for removing fixed-value impulse noise from grayscale images. J Real Time Image Process 2018;14:617-33. doi: 10.1007/s11554-017-0746-8.
- Hashem NM, Abbas HK, Mohamad HJ. Optical System to Recognize Car Plate Ownership. Malays J Fundam Appl Sci 2023;19:406-16. doi: 10.11113/mjfas.v19n3.2991.
- Yim J, Sohn K. Enhancing the Performance of Convolutional Neural Networks on Quality Degraded Datasets. [Online] 2017 [Cited 2024 August 24]. Available from URL: https://arxiv.org/pdf/1710.06805
- Touma TA, Abbas HK, Mohamad HJ, Al-Zuky AA. Intelligent detection of traffic lights using morphological operations. AIP Conf Proc 2023;2475:090020. doi: 10.1063/5.0102888.
- Ashour AS, Beagum S, Dey N, Ashour AS, Pistolla DS, Nguyen GN et al. Light microscopy image de-noising using optimized LPA-ICI filter. Neural Comput Appl 2018;29:1517-33. doi: 10.1007/s00521-016-2678-9.
- Abtan RA, Al-Saleh AH, Mohamed HJ, Abbas HK, Alzuky A. Texture Features of Grey Level Size Zone Matrix for Breast Cancer Detection. Iraqi J Sci 2023;64:492-502. doi: 10.24996/ijs.2023.64.1.43.
- Kumar SN, Fred AL, Varghese PS. An overview of segmentation algorithms for the analysis of anomalies on medical images. J Intell Syst 2019;29:612-25. doi: 10.1515/jisys-2017-0629.
- Gao Z. An Adaptive Median Filtering of Salt and Pepper Noise based on Local Pixel Distribution. In: Proceedings of the 2018 International Conference on Transportation & Logistics, Information & Communication, Smart City (TLICSC 2018). 2018. Doi: 10.2991/tlicsc-18.2018.77.
- Resham NH, Abbas HK, Mohamad HJ, Al-Saleh AH. Noise reduction, enhancement and classification for sonar images. Iraqi J Sci 2021;62:4439-52. Doi: 10.24996/ijs.2021.62.11(SI).25.
- Abbas HK, Al-Saleh AH, Mohamad HJ, Al-Zuky AA. New algorithms to enhanced fused images from auto-focus images. Baghdad Sci J 2021;18. doi: /10.21123/bsj.2020.18.1.0124.
- Ajay, Brijendra, Department, Engineering C, Military, Military, et al. A Review Paper: Noise Models in Digital Image Processing. arXiv pre-print server. 2015.
- Jawad EM, Hazim HJ, Daway G. Retinal image enhancement by using adapted histogram equalization based on segmentation and lab color space. Int J Intell Eng Syst 2022;15:614-22. doi: 10.22266/ijies2022.0630.52.
- Diwakar M, Lamba S, Gupta H. CT image denoising based on thresholding in shearlet domain. Biomed Phaemacol J 2018;11:671-7. doi: 10.13005/bpi/1420.

 Choi H, Jeong J. Speckle noise reduction for ultrasound images by using speckle reducing anisotropic diffusion and Bayes threshold.
 J Xray Sci Technol 2019;27:885-98. doi: 10.3233/XST-190515.
 PMID: 31256113.

- Duarte-Salazar CA, Castro-Ospina AE, Becerra MA, Delgado-Trejos E. Speckle noise reduction in ultrasound images for improving the metrological evaluation of biomedical applications: an overview. IEEE 2020;8:15983-99. doi: 10.1109/ACCESS.2020.2967178.
- Singh K, Ranade SK, Singh C. A hybrid algorithm for speckle noise reduction of ultrasound images. Comput Methods Programs Biomed 2017;148:55-69. doi: 10.1016/j.cmpb.2017.06.009.
- Park J, Kang JB, Chang JH, Yoo Y. Speckle reduction techniques in medical ultrasound imaging. Biomed Eng Lett 2014;4:32-40. doi: 10.1007/s13534-014-0122-6.
- Gelas C, Villard L, Ferro-Famil L, Polidori L, Koleck T, Daniel S. Multi-Temporal Speckle Filtering of Polarimetric P-Band SAR Data over Dense Tropical Forests: Study Case in French Guiana for the BIOMASS Mission. Remote Sens 2021;13:142. doi: 10.3390/rs13010142.
- Dalsasso E, Yang X, Denis L, Tupin F, Yang W. SAR image despeckling by deep neural networks: From a pre-trained model to an end-to-end training strategy. Remote Sens 2020;12:2636. doi: 10.3390/rs12162636.
- Tounsi Y, Kumar M, Nassim A, Mendoza-Santoyo F. Speckle noise reduction in digital speckle pattern interferometric fringes by nonlocal means and its related adaptive kernel-based methods. Appl Opt 2018;57:7681-90. doi: 10.1364/AO.57.007681.
- Gomez L, Ospina R, Frery AC. Statistical properties of an unassisted image quality index for SAR imagery. Remote Sens 2019;11:385. doi: 10.3390/rs11040385.
- Huang Y, Li W, Yuan F. Speckle noise reduction in sonar image based on adaptive redundant dictionary. J Mar Sci Eng 2020;8:761. doi: 10.3390/jmse8100761.
- Wang T, Ma L, Qi Q. Application of Remote Sensing Image in Civil Engineering. E3S Web Conf 2020;206:01003. doi: 10.1051/e3sconf/202020601003.
- Mahendra HN, Mallikarjunaswamy S, Siddesh GK, Komala M, Sharmila N. Evolution of real-time onboard processing and classification of remotely sensed data. J Sci Technol 2020;13:2010-20. doi: 10.17485/IJST/v13i20.459.
- Golilarz NA, Mirmozaffari M, Gashteroodkhani TA, Ali L, Dolatsara HA, Boskabadi A, et al. Optimized wavelet-based satellite image de-noising with multi-population differential evolution-assisted harris hawks optimization algorithm. IEEE Access 2020;8:133076-85. doi: 10.1109/ACCESS.2020.3010127.
- Arienzo A, Argenti F, Alparone L, Gherardelli M. Accurate despeckling and estimation of polarimetric features by means of a spatial decorrelation of the noise in complex PolSAR data. Remote Sens 2020;12:331. doi: 10.3390/rs12020331.
- Abbas H, Ahmad S. Statistical analysis of medical image fusion techniques based on edge detection. Advances in Natural and Applied Sciences 2017;11:268-77.

Open Access Vol. 74, No.10 (Suppl. 8), October 2024